ISSN : 0974 - 7435 Volume 10 Issue 20

2014

BioTechnology

An Indian Journal

FULL PAPER

BTAIJ, 10(20), 2014 [12117-12125]

Bounded error segmentation algorithm and focusing delay generation

Wang Ping[1,*], Wang Siqi[1], Wang Linhong[2], Cheng Na[1], Gong Zhihui[1], Pan Zhen[1]
[1]Department of Electrical and Electronics Engineering, Chongqing University, Chongqing, 400044, (CHINA)
[2]Department of Applied Electronics, Chongqing College of Electronic Engineering, Chongqing 401331, (CHINA)
E-mail: cqu_dqwp@163.com

ABSTRACT

The highly efficient and real-time generation of focusing delays in dynamic focusing systems is always difficult to implement. This paper proposes a segmentation method for dynamic focusing on the basis of bounded error, as well as a scheme for compressing and generating focusing delays. The segmentation boundaries satisfying the restricting error and the corresponding focusing delays in the segmentation depth can be calculated according to the number of focusing channels, the sampling frequency, and the given bounded error. Moreover, the quantization units are dynamically changed to reduce further the errors in the focusing delays of each channel. Finally, schemes for compressing and generating focusing delays are proposed. The numerical analysis and experimental results indicate that the proposed approach can obtain the least number of segmentations under the bounded error in the detecting range and significantly reduce the memory requirement of focusing delays. The SSIM of generated images by using the proposed approach and ideal dynamic focus is 0.948.

KEYWORDS

Ultrasound imaging; Dynamic focusing; Bounded error; Focusing delays.

INTRODUCTION

In dynamic focusing systems, signals of the destination reflectors are obtained by summing the echo signal of each channel after a series of specific delays[1,2]. To improve the lateral resolution of images, the technology of dynamic focusing is generally implemented by hardware systems directly; however, real-timely generating the focusing delays for each channel is always difficult to be implemented[3]. In most of ultrasound systems, two mainstream methods are introduced to generate focusing delays. One mainly involves calculating real-time focusing delays directly, which depends on FPGA's strong ability in calculation, and the other involves storing compressed focusing delay data. The former method generally uses the Coordinate Rotation Digital Computer (CORDIC) algorithm or recursive algorithm to avoid complex squaring and rooting operations. However, as the number of focusing channels increases, the method consumes a significant amount of FPGA resources[4]. Obviously it will lead to the high cost of hardware. The latter method mainly generates focusing delays by decompressing compressed focusing delays which are pre-stored as reference data sets. These algorithms can avoid the direct storage of focusing delays and thus reduce memory requirements[5], but the approaches often lead the peripheral circuit of the latter algorithm to be very complicated, and correspondingly the hardware consumption would become very large when the dynamic focusing system has 64 or 128 channels[6–9]. For example, the ultrasound system of the Philips HD7 series has taken pixel-level dynamic focusing technology and the fine ash-step point using point focusing technology, and the number of focusing channels reached up to 1,024 channels in Philips HD7 series products. In such case, high-quality digital beamforming is essential to high-end ultrasound systems, and the high-quality digital beamforming always requires the generation of focusing delays in a highly efficient and simple manner. Thus, real-time and highly efficient generation algorithms for multi-channel, high-precision focusing delays are worth studying.

This paper proposes a method for obtaining the least number of segmentations according to the given bounded error. Meanwhile, it presents a high efficient scheme for generating focusing delays. In order to test the effectiveness of the proposed method, focusing error analysis and point target imaging experiments are conducted.

The remainder of this paper is organized as follows. Section II analyzes the theorem of dynamic focusing. Section III proposes the segmentation algorithm of dynamic focusing based on the given bounded error and the schemes for compressing and generating focusing delays. Section IV shows the numerical analysis and experimental results. Section V draws a conclusion.

DYNAMIC FOCUSING

In the receiving process, focusing delays of dynamic focusing always change as focal depth increases[10]. Ideally, all points of each scan line continue to serve as focal points in the process of dynamic focusing. To accomplish this task, the dynamic focusing system must trace targets along the scan line according to the speed of echo signals.

If reference origin O is the center of the linear subarray, then the coordinate of the i-th element of the linear subarray is

$$x_i = \left(i - \frac{N+1}{2}\right)d, \quad 1 \le i \le N \tag{1}$$

Where N is the number of linear subarray elements, i is the ordinal number of elements, and d is the center interval of array elements. Figure 1 presents the coordinate of i-th and j-th elements.

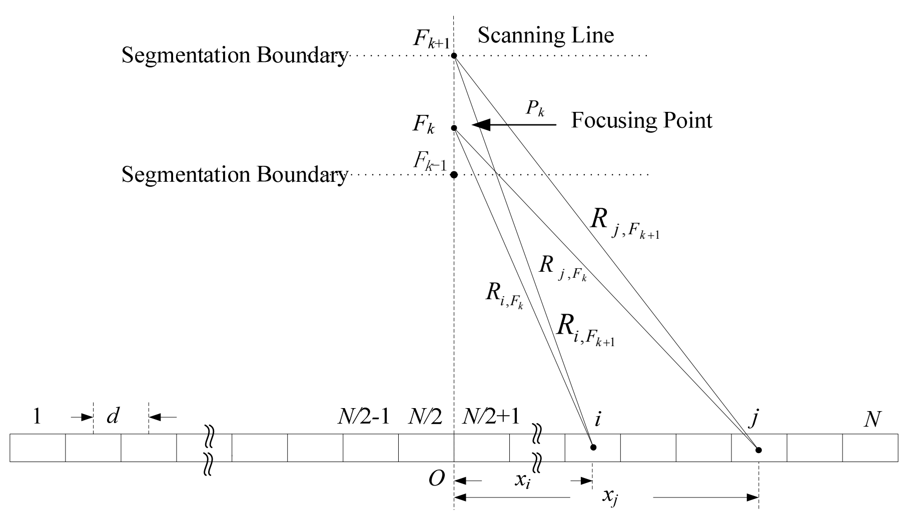

Figure 1 : Calculation of focusing delays of the linear subarray

where F_k is focal depth at the focusing point P_k, R_{i,F_k} is the distance from the i-th element to the focusing point P_k, and the reference origin O is the center of the linear subarray. The acoustic-path difference $\Delta R_{i,F_k}$ is

$$\Delta R_{i,F_k} = R_{i,F_k} - F_k = \sqrt{F_k^{\,2} + x_i^{\,2}} - F_k \qquad \text{(2)}$$

The delay data τ_{i,F_k} can be obtained as follows

$$\tau_{i,F_k} = \Delta R_{i,F_k} / c = \frac{1}{c}(\sqrt{F_k^{\,2} + x_i^{\,2}} - F_k) \qquad \text{(3)}$$

where c is the ultrasound speed.

The delay and sum beamforming S_{DAS} at the focusing point P_k can be calculated as follows

$$S_{DAS} = \sum_{i=1}^{N} s(t - \frac{F_k}{c} - \tau_{i,F_k}) \qquad \text{(4)}$$

The minimum interval between two adjacent focal points ΔF, focusing number N_p, the necessary number of focusing delays M_s, and the maximum data bandwidth B_w can be calculated as follows[11]

$$\begin{cases} \Delta F = c/(2f_s) \\ N_p = 2F_L f_s / c \\ M_s = mN_p/2 = mF_L f_s / c \\ B_w = mf_s \end{cases} \qquad \text{(5)}$$

where f_s is the sampling rate, m is the number of elements, and F_L is the depth of detection.

When the detection depth F_L is 240 mm and the sample rate f_s is 50 MHz, the number of focusing delays N_p is 1.56×10^4. For a modest ultrasound system with a 32-channel, 128-element transducer, the symmetry in the beamforming can be exploited, such that the number of values is halved. In this case, if a focusing delay serves as 2 bytes, the necessary number of focusing delays M_s can reach up to 4.98×10^5 bytes and the maximum data bandwidth B_w is 1,600 Mbytes/s. In such cases, a single-chip such as FPGA with limited memory could hardly fit with the dynamic focusing circuits[12].

DYNAMIC FOCUSING SEGMENTATION AND FOCUSING DELAYS OPTIMIZATION

Dynamic focusing segmentation

Segmentation algorithm of dynamic focusing based on bounded error

The linear subarray is shown in Figure 1. The delay profiles are symmetrical and thus allow the subarray to be halved. Moreover, only the elements $N/2+1$ to N (N is even) are considered.

According to (2) and (3), when the focal depth changes from F_k to F_{k+1}, the deviations of focusing delays $\Delta\tau_i$ and $\Delta\tau_j$ can be calculated as follows.

$$\begin{cases} \Delta\tau_i = \tau_{i,F_k} - \tau_{i,F_{k+1}} = \frac{1}{c}[(\sqrt{F_k^2 + x_i^2} - \sqrt{F_{k+1}^{\,2} + x_i^2}) - (F_k - F_{k+1})] \\ \Delta\tau_j = \tau_{j,F_k} - \tau_{j,F_{k+1}} = \frac{1}{c}[(\sqrt{F_k^2 + x_j^2} - \sqrt{F_{k+1}^{\,2} + x_j^2}) - (F_k - F_{k+1})] \end{cases} \qquad \text{(6)}$$

According to (6), the relations between $\Delta\tau_i$ and $\Delta\tau_j$ can be obtained.

$$|\Delta\tau_j| > |\Delta\tau_i|,\ j>i \text{ and } i, j \in [N/2+1, N] \qquad \text{(7)}$$

Where $i, j \in [N/2+1, N]$, $j>i$, and $x_j > x_i$.

According to (7), in the range of focal depth $[F_k, F_{k+1}]$, if $|\Delta\tau_N| < \delta$, (8) can be established.

$$|\Delta\tau_{N/2+1}| < \cdots < |\Delta\tau_i| < \cdots < |\Delta\tau_j| < \cdots < |\Delta\tau_N| < \delta \qquad \text{(8)}$$

In particular, if the focusing delay error $\Delta\tau_N$ is under the given bounded error δ, the focusing delay errors of other elements will not exceed δ.

Therefore, in the detection range [F_0, F_L], segmentation positions or focusing points can be calculated according to (9).

$$\begin{cases} \tau_{N,F_{k-1}} - \tau_{N,F_k} = \delta \\ \tau_{N,F_k} - \tau_{N,F_{k+1}} = \delta \\ F_{k-1} < F_k < F_{k+1} \\ k \geq 1 \\ F_{k+1} \leq L \end{cases} \tag{9}$$

where τ_{N,F_k} is the focusing delay of N-th element at focal point P_k. Figure 1 shows that if each channel is beamformed according to focusing delays [$\tau_{1,F_k}, \tau_{2,F_k}, ..., \tau_{N,F_k}$] at focal point P_k, then the focusing error will be less than δ in the detection range [F_{k-1}, F_{k+1}].

According to (3) and (9), F_k can be derived as follows

$$\begin{cases} F_k = \dfrac{{x_N}^2 - l^2}{2l} \\ l = c \cdot (\tau_{N,F_{k-1}} - \delta), \quad k = 1, 2, ..., K \end{cases} \tag{10}$$

where τ_{N,F_0} can be calculated using (3). According to (10), F_1, F_2,..., F_k can be sequentially calculated in the detection range [F_0,F_L], where F_0, F_2, F_4,..., F_K are segmentation boundaries, and F_1, F_3, F_5,..., F_{K-1} are the focusing points of the corresponding segmentations.

The focusing number FN_s at the s-th segmentation boundaries can be obtained as follows

$$FN_s = 2F_{2s}f_s/c, \ (s=0,1,\ldots,K/2) \tag{11}$$

The least segmentations number S_{min} in the detection range [F_0, F_L] can be calculated as follows.

$$S_{min} = (\tau_{N,F_0} - \tau_{N,F_K}) / 2\delta \tag{12}$$

Where δ is the bounded error. If the segmentation number is less than S_{min}, the expression (9) cannot be established. Thus, the number of segmentations derived by (12) will be the least if the bounded error and detection range are given.

Optimal approximating algorithm of the dynamic focusing delays

In dynamic focusing systems, the element closer to the focusing center line has a stronger influence of the echo signal on the beamforming. According to (3) and (4), when the focusing depth is the same and the bounded error is given, the closer the focusing channels to the focusing center line are, the smaller the delays value of the channels are and the larger the relative errors are. To improve the accuracy of beamforming further, the dynamic approximation unit λ_i is introduced for focusing channels as follows.

$$\begin{cases} \lambda_i = \delta & (\dfrac{3N}{4} < i \leq N) \\ \lambda_i = \dfrac{\delta}{2} & (\dfrac{5N}{8} < i \leq \dfrac{3N}{4}) \\ \lambda_i = \dfrac{\delta}{4} & (N/2 + 1 \leq i \leq \dfrac{5N}{8}) \end{cases} \tag{13}$$

Dynamic focusing segmentation and focusing delays optimization

The detection depth is 2 mm–240 mm, according to (1), (3), (9), and (10). The segmentation number S is 82.

Figure 2 (a) shows the stair-step approximation of the segmentation focusing delays, which is based on the unified approximation unit. Figure 2 (b) is the high-precision approximation for focusing delays, which is based on dynamic approximation unit.

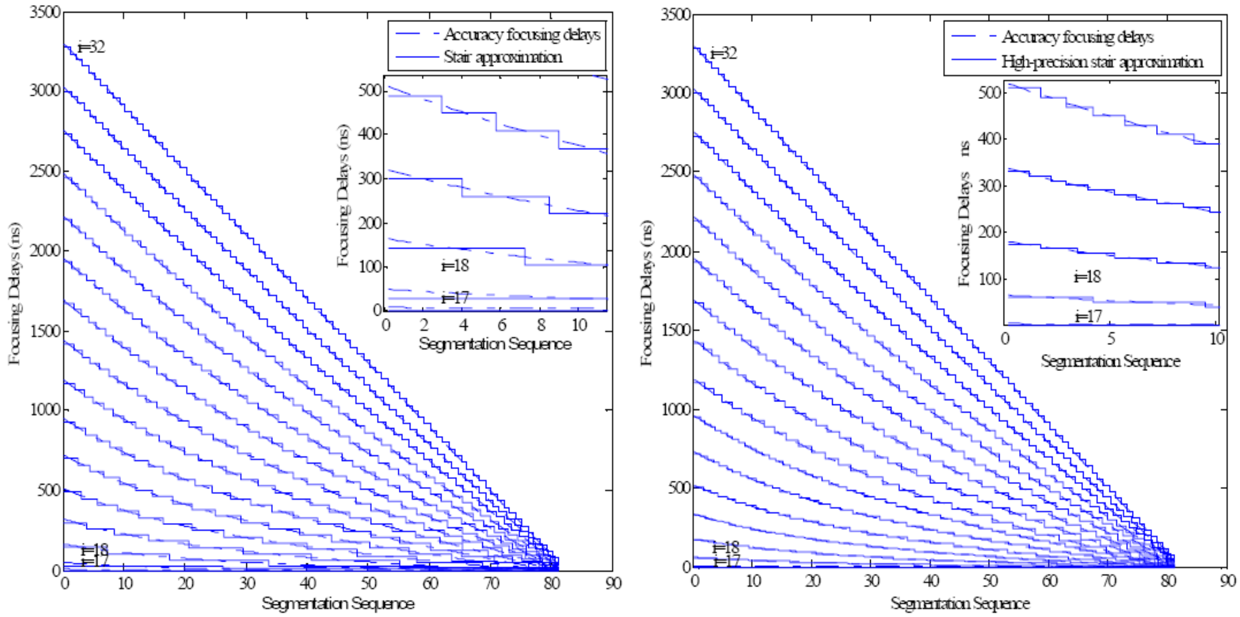

(a) Stair-step approximation for focusing delays (b) High-precision stair-step approximation for focusing delays

Figure 2 : The comparison of approximation for focusing delays

Figure 2 (a) and (b) show that the ideal focusing delays are always surrounded by approximate focusing delays, and the maximum error is limited within the same approximation unit. Compared with the upper right corner of Figure 2 (a) and (b), the introduction of dynamic approximation unit λ_i can minimize the relative errors for the focusing channels, which are closer to the focusing center line. This innovation is beneficial for improving the quality of scanning lines.

Compression storage of the focusing delays

The focal depth increases, ideal focus delays become a smooth curve. To approximate the ideal focusing delays, the i-th channel and s-th segmentation focusing delays $T_{i,s}$ can be corrected according to (14) in real time.

$$T_{i,s} = \begin{cases} T_{i,s\text{-}1}, & |T_{i,s-1} - \tau_{i,s}| < \lambda_i \\ T_{i,s\text{-}1} - \lambda_i, & |T_{i,s-1} - \tau_{i,s}| \geq \lambda_i \end{cases} \qquad s = 1, 2, \ldots, S \tag{14}$$

Figure 3 shows the relationship between the stair-step approximation and the accuracy focusing delays curve of the i-th channel.

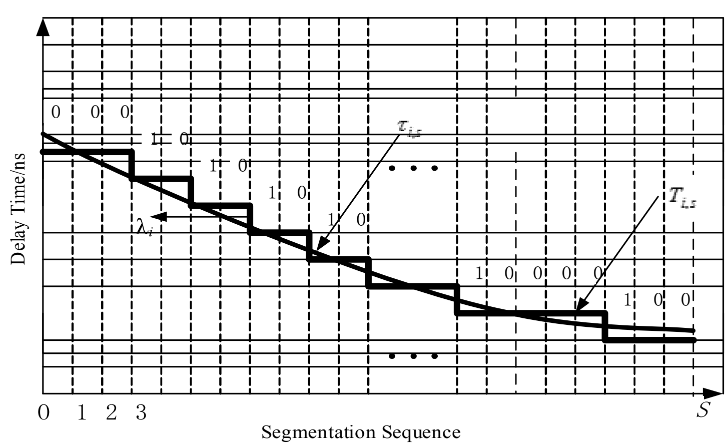

Figure 3 : The stair line approximates to focusing delays

In the graph, the horizontal axis is the segmentation number, the vertical axis is the value of focusing delays, and λ_i is the approximation unit.

Figure 3 shows that the stair-step approximation of focusing delays $T_{i,s}$, which is corrected according to the approximation information $BIT_{i,s}$ (approximation information of i-th element and s-th segmentation) in real time and can also be presented as (15).

$$BIT_{i,s} = \begin{cases} 1, & |T_{i,s\text{-}1} - \tau_{i,s}| \geq \lambda_i \\ 0, & |T_{i,s\text{-}1} - \tau_{i,s}| < \lambda_i \end{cases} \quad \textbf{(15)}$$

When the difference between $T_{i,s}$ and $\tau_{i,s}$ is larger than λ_i, the corresponding approximation information $BIT_{i,s}$ can be represented as 1 and the stair-like line $T_{i,s}$ must be decreased by λ_i. Otherwise, $BIT_{i,s}$ is 0, and $T_{i,s}$ retains its value. Thus, according to (14) and (15), the focusing delays $T_{i,s}$ can be corrected by the λ_i in real time to approximate the ideal focusing delays $\tau_{i,s}$.

Generation of dynamic focusing delays

Considering the above approach, which uses stair-line to approximate the ideal focusing delays curve, Figure 4 presents the scheme of focusing generation delays for 32 channels.

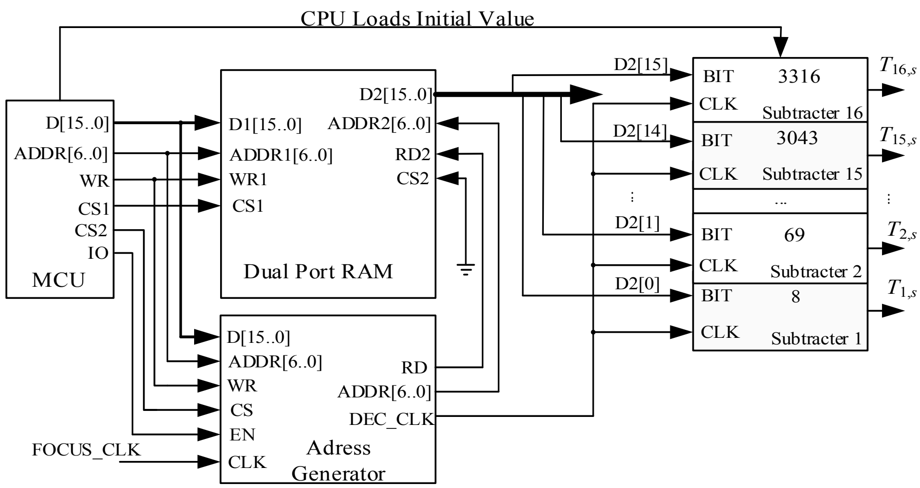

Figure 4 : The scheme of focusing delays' generator

Before the generation of focusing delays, the MCU loads the approximation information $BIT_{i,s}$ of the segments to the dual port RAM, the focusing number FN_s (s=0,1,…,81) to the address generator, as well as the initial value $T_{i,0}$ ($T_{i,0}$ is the i-th channel's focusing delay of the first segmentation) and the approximate unit λ_i (the approximate unit of i-th channel) to the corresponding subtracter. When the dynamic focusing starts, the address generator counts the FOCUS_CLK. If the counted value is equal to the focusing number FN_s, the address generator increases the ADDR[6..0] by 1, and the dual port RAM outputs the approximation information $BIT_{i,s}$ of the next segment to the subtracters. If the $BIT_{i,s}$ is 1, $T_{i,s}$ is decreased by λ_i. Thus, $T_{i,s}$ can be generated in real time. Figure 3 shows the approximation process of $T_{i,s}$.

ANALYSES AND EXPERIMENT

Memory requirement calculation and comparison

The initial value of the focusing delays of each channel requires 2 bytes to store. Given the symmetry of the linear subarray, the memory requirement M_1 of focusing delays of N channels is

$$M_1 = (N/2) \times 2 = 32\text{bytes}$$

The memory requirement of λ_i is a byte, and the memory requirement M_2 of N channels is

$$M_2 = (N/2) \times 1 = 16\text{bytes}$$

The memory requirement of each focusing number FN_s, which records the segmentation boundaries, is 2 bytes. The memory requirement M_3 of all focusing numbers is

$$M_3 = S \times 2 = 164\text{bytes}$$

The memory requirement of the focusing delay approximation information $BIT_{i,s}$ of each channel in each segmentation is a binary bit. The memory requirement M_4 of N channels is

$$M_4 = S \times N / 2 / 8 = 164\text{bytes}$$

Thus, only M_1+M_2+M_3+M_4=376 bytes can reconstruct the segmentation focusing delay $T_{i,s}$. TABLE 1 presents the comparison of memory requirement of different numbers of channels between the direct storage with the proposed algorithm in this study, where the bounded error δ is 20 ns.

TABLE 1 : Comparison of memory requirement about different focusing methods

Focusing beamforming type	**memory requirement (Bytes)**		
	32-channel	**64- channel**	**128-channel**
Ideal dynamic focusing beamforming	494560	989120	1978240
Proposed dynamic focusing beamforming	376	1230	3472
Compression ratio	1/1315	1/804	1/570

TABLE 1 shows that in 32-channel focusing system, the compression ratio can reach up to 1/1315. Although the compression ratio decreases as the number of channels increases, the compression ratio for 128-channel focusing system is 1/570. Apparently, the proposed segmentation method can save a significant amount of memory for dynamic focusing delays.

Error analysis of optimized approximation

The ultrasonic echo signal is defined as $s_0 = \sin(2\pi f_0 t + \varphi_0)$, where φ_0 is the initial phase. The ideal delay and sum beamforming for 32 channels is

$$s_1 = 32 s_0 = 32\sin(\omega t + \varphi_0) \tag{16}$$

For ultrasonic echo signals with 3.5 MHz, the maximum phase error □ is 0.4398 rad when the bounded error δ is 20 ns. According to (13), the delay and sum beamforming for 32 channels based on the proposed algorithm is

$$s_2 = 2[\sum_{z=17}^{20}\sin(\omega t + \varphi_0 + \varphi_z / 4) + \sum_{z=21}^{24}\sin(\omega t + \varphi_0 + \varphi_z / 2) + \sum_{z=25}^{32}\sin(\omega t + \varphi_0 + \varphi_z)] \tag{17}$$

where φ_z is the random distribution during $[-\varphi,\varphi]$. Figure 5 presents the waveforms of s_1 and s_2.

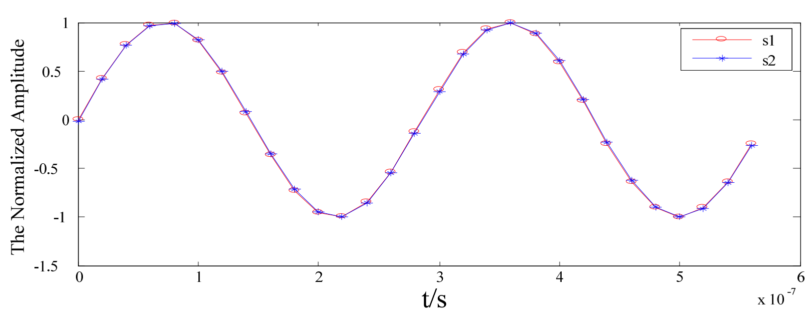

Figure 5 : Comparison of different beamforming methods

Figure 5 shows that when the bounded error δ is 20 ns, signals s_1 and s_2 basically coincide. The further comparison indicates that the correlation coefficient of s_1 and s_2 is 0.9999, and the PRD (percentage root mean squared difference)[13] of s_1 and s_2 is 0.0276%.

Point target imaging experiment

The simulation uses fixed-point emission and 32-channel and 128-element linear array transducers. The center interval d of array elements is 0.44 mm. The emission frequency f_0 is 3.5 MHz, the emission focal point is at 50 mm, the sampling frequency f_s is 50 MHz, and the ultrasound velocity c is 1,540 m/s. The analysis and simulation are implemented using MATLAB 7.10.

The point scattering target experiment is implemented using Field II[14]. Then, 60 dB Gaussian white noise is added to the ultrasonic signal[15], and the dynamic range of imaging is 60 dB. The six target scattering points are located at (0 0 30), (0 0 40), (0 0 50), (0 0 60), (0 0 70), and (0 0 80) mm, and the detection width is 10 mm. The simulation results are shown in Figure 6. Figure 6 (a) shows the imaging simulation of ideal dynamic focusing, and Figure 6 (b) is the imaging simulation of proposed segmentation dynamic focusing. Compared with Figure 6 (a), Figure 6 (b) shows that the images simulated using the proposed method and the ideal dynamic focusing are basically the same, and the structural similarity index Structural Similarity index (SSIM)[16] in Figure 6 (a) and (b) is 0.948.

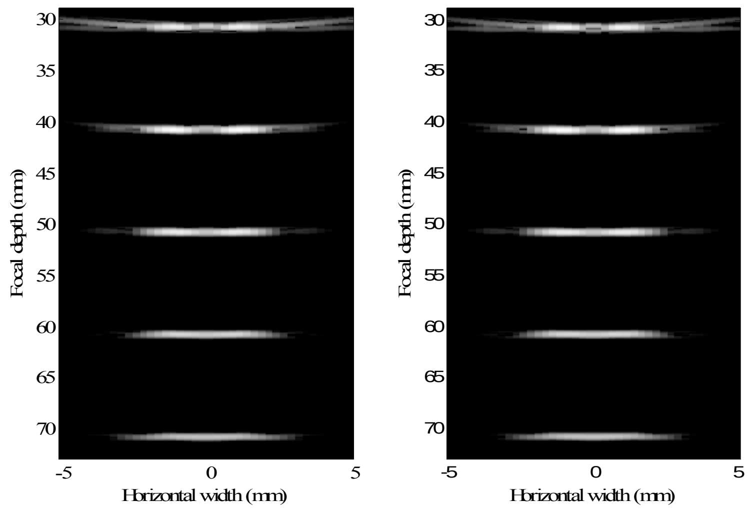

(a) Ideal dynamic focusing (b) Segmentation dynamic focusing

Figure 6 : Comparison of different imaging simulations

TABLE 2 : Performance of point targets

Number	Point targets/mm	ρ	PRD (%)	SSIM
1	(0,0,30)	0.9862	2.57	0.9726
2	(0,0,40)	0.9879	2.42	0.9853
3	(0,0,50)	0.9891	2.16	0.9764
4	(0,0,60)	0.9977	0.47	0.9721
5	(0,0,70)	0.9967	0.66	0.9870
6	(0,0,80)	0.9789	2.61	0.9846

TABLE 2 shows that the correlation coefficients of the six target points are more than 0.97, the maximal PRD is less than 3%, and the minimal SSIM is more than 0.970. The images simulated using the proposed method and ideal dynamic focusing are highly consistent.

CONCLUSION

(1) This paper proposes a segmentation method for dynamic focusing based on bounded error and the generation focusing delay scheme. The core idea of the proposed method is segmenting the detection depth based on the bounded error δ of focusing delays and constraining the error of focusing delays within the given bounded error δ in the whole detection range. The accuracy of delays of each focusing channel is enhanced by dynamically changing the approximation unit λ_i.

(2) The corresponding compressed storage method and real-time generation schemes for focusing delays are proposed in this paper. The proposed method can avoid complex multiplications and significantly improve the compression ratio of focusing delays. It also provides an efficient method to generate focusing delays for high-end digital ultrasonic imaging system.

(3) Error analysis, the point target imaging experiment, and similarity analysis show that the images simulated using the proposed method and those simulated through ideal dynamic focusing are basically the same. In addition, to meet different precision requirements, the proposed method can provide a good tradeoff between the compression ratio and memory consumption by adjusting the given bounded error δ.

(4) The proposed method avoids complex multiplications and significant reduces the storage capacity of the focusing delays. These advantages make realizing a multi-channel and high-precision dynamic focusing system with a single low capacity FPGA possible.

ACKNOWLEDGEMENT

This work is supported by Project No. CDJZR11 15 00 04 from the Fundamental Research Funds for the Central Universities and the National Science Foundation Project of CQ CSTC2012JJA10129.

REFERENCES

[1] J.P.Asen, A.Austeng, S.Holm; "Capon beamforming and moving objects-an analysis of lateral shift-invariance", IEEE Transactions on Ultrasonics Ferroelectrics and Frequency Control, **61**, 1152-60, **(July 2014)**.

[2] C.H.Yoon, Y.M.Yoo, T.K.Song, J.H.Chang; "Pixel based focusing for photoacoustic and ultrasound dual-modality imaging", Ultrasonic, **54**, 2126-33 **(August 2014)**.

[3] E.Filoux, A.Sampathkumar, P.V.Chitnis, O.Aristizabal, J.A.Ketterling; "High-frequency annular array with coaxial illumination for dual-modality ultrasonic and photoacoustic imaging, Review of scientific instruments", **(84)**, 053705 **(May 2013)**.

[4] W.H.Yu, C.F.Cheang, P.I.Mak, et al; "A nonrecursive digital calibration technique for joint elimination of transmitter and receiver I/Q imbalances with minimized add-on hardware, IEEE Transactions on Circuits and Systems II-express Briefs", **60**, 462-466 **(August 2013)**.

[5] S.I.Nikolov, J.A.Jensen, B.Tomov; "Recursive delay calculation unit for parametric beamformer. in Proc. SPIE Progress in Biomedical Optics and Imaging", **6147**, 6147D-1–6147D-12, **(2006)**.

[6] Z.X.Zhao, T.Xiang, M.Gao, et al; "A Pipelined Beamforming Delay Calculation Architecture in Ultrasound Imaging System", June 10-12, Shanghai, Chinese: Computer Science and Automation Engineering (CSAE), 2011 IEEE International Conference on: 162-166 **(2011)**.

[7] D.Lertsillp, S.Umchid, U.Techavipoo, P.Thajchayapong; "Resolution improvements in ultrasound elastography using dynamic focusing", Biomedical Engineering International Conference (BMEiCON), 225-228 **(2011)**.

[8] G.T.Borislav, A.J.Jorgen; "Delay generation methods with reduced memory requirements", Ultralsonic Imaging and Signal Processing, **5035**, 491-500 **(2003)**.

[9] S.I.Nikolov, J.A.Jensen, B.G.Tomov; "Fast parametric beamformer for synthetic aperture imaging", IEEE Transactions on Ultrasonic Ferroelectrics and Frequency Control, **55**, 1755-1767, **(August 2008)**.

[10] J.A.Jensen, H.Holten-Lund, R.T.Nilsson, et al; "SARUS: A synthetic aperture real-time ultrasound system", IEEE Transactions on Ultrasonic Ferroelectrics and Frequency Control, **60**, 1838-1852, **(Sep 2013)**.

[11] D.Lertsillp, S.Umchid, U.Techavipoo, P.Thajchayapong; "Resolution improvements in ultrasound elastography using dynamic focusing", Biomedical Engineering International Conference (BMEiCON), 1-4 **(2012)**.

[12] A.A.Assef, J.M.Maia, F.K.Schneider, V.L.S.N.Button, E.T.Costa; "A reconfigurable arbitrary waveform generator using PWM modulation for ultrasound research", Biomedical Engineering online, **24**, 1-13 **(Dec 2013)**.

[13] A.Mishra, F.Thakkar, C.Modi, R.Kher; "ECG signal compression using Compressive Sensing and wavelet transform", Engineering in Medicine and Biology Society (EMBC), 2012 Annual International Conference of the IEEE., 3404-3407 **(2012)**.

[14] L.P.Wong Lawrence, I.H.Chen Albert, Z.H.Li, S.Logan Andrew, T.W.Yeow John; "A row-column addressed micromachined ultrasonic transducer array for surface scanning applications", Ultrasonics, **54**, 2072-2080 **(August 2014)**.

[15] A.J.Casper, D.Liu, J.R.Ballard, E.S.Ebbini; "Real-time implementation of a dual-model ultrasound array system: in vivo results", IEEE Transactions on Biomedical Engineering, **60**, 2751-2759 **(Oct 2013)**.

[16] W.Zhou, C.B.Alan, R.S.Hamid, P.S.Eero; "Image quality assessment: From error visibility to structural similarity", IEEE Transactions on Image Processing, **13**, 600-612 **(Apr 2004)**.